Reac Kinet Mech Cat (2016) 117:745–759
DOI 10.1007/s11144-015-0963-8

Mesoporous metal(IV) phosphates as high performance acid catalysts for the synthesis of photochromic bis-naphthopyran via Claisen rearrangement

Abd El Rahman S. Khder[1,2] · **Saleh A. Ahmed**[1,3] · **Hatem M. Altass**[1]

Received: 17 August 2015 / Accepted: 30 November 2015 / Published online: 15 December 2015

Abstract In this work, a facile and efficient one-step method for the synthesis of highly active mesoporous zirconium and tin(IV) phosphate that exhibit excellent catalytic activity for the synthesis of photochromic bis-naphthopyran via the Claisen rearrangement has been established. The synthesized catalysts were characterized by different textural and spectroscopic techniques such as XRD, FTIR spectra, SEM, TEM and N_2 adsorption–desorption at −196 °C. The surface acidity of the prepared catalysts were determined by nonaqueous potentiometric titration with n-butylamine and FTIR of chemisorbed pyridine. XRD and N_2 adsorption–desorption measurements showed that, the samples have some mesoporous structure. The surface acidity measurement showed that the samples contain mixture of Lewis and Brønsted acid sites. The results showed that zirconium phosphate samples have higher surface acidities than tin phosphate samples, and the samples with Zr:P ratio 1:3 and Sn:P ratio 1:2 showed the highest surface and Brønsted acidities. The prepared catalysts showed excellent catalytic activity for the synthesis of photochromic bis-naphthopyran via the Claisen rearrangement. High yield (∼99 %) with 100 % selectivity of photochromic bis-naphthopyran was obtained in shorter reaction time at room temperature. These acid catalysts may solve the problematic

Electronic supplementary material The online version of this article (doi:10.1007/s11144-015-0963-8) contains supplementary material, which is available to authorized users.

✉ Abd El Rahman S. Khder
askhder2244@yahoo.com

Saleh A. Ahmed
saleh_63@hotmail.com

[1] Chemistry Department, Faculty of Applied Science, Umm Al Qura University, Mecca, Saudi Arabia

[2] Chemistry Department, Faculty of Science, Mansoura University, Mansoura, Egypt

[3] Chemistry Department, Faculty of Science, Assiut University, Asyût 71516, Egypt

low yield and purification difficulties of the photochromic chromenes reported previously.

Keywords Tin phosphate · Zirconium phosphate · Surface acidity · Photochromic chromenes · Claisen rearrangement

Introduction

In recent years, environmental considerations have raised strong interest in the development of economically feasible materials and processes to eliminate the use of harmful substances and the generation of toxic waste materials. In this respect, heterogeneous catalysis can play a key role in the development of environmentally benign processes particularly in the petroleum and chemical industries. For example, sulfuric and fluorohydric acids are commonly used in many industrial chemical processes that involve alkylation, esterification, hydrolysis, and other chemical reactions [1–3]. However, these acid catalysts are toxic, corrosive and most importantly, difficult to remove from the reaction medium. Solid acid catalysts are particularly important in acid catalyzed reactions as a safe alternative to the hazardous and corrosive materials such as HF, sulfuric and nitric acid [4, 5]. Day by day, a lot of efforts have been made to develop the recoverable solid acid catalysts for minimizing pollution and reducing cost [4–7].

Metal phosphates are one of the most important classes of inorganic materials used for a wide range of applications [8]. Metal phosphates have the general formula $M^{IV}(HXO_4)_2{\cdot}nH_2O$ where M^{IV} = Sn, Ti, Zr, Ce, and X = P, As, W, Mo. These materials behave as cation exchangers due to the presence of exchangeable protons contained in structural hydroxyl groups. Moreover, they possess both Brønsted and Lewis acid sites combined with thermal stability. So, these compounds have been reported as solid acid catalysts for different organic reactions [9, 10].

Studies have been carried out to determine the acidic properties of these catalysts [11]. Studies have shown that the amorphous form of these catalysts demonstrate higher activity due to increased overall acidity and surface area compared to their crystalline analog [12, 13]. Moreover, metal(IV) phosphates are beneficial as catalyst supports for metal oxides due to their textural and acid properties [14, 15]. Hattori et al. have investigated the source of the active sites on this class of catalysts. In their study of crystalline zirconium phosphate, he concluded that the catalyst possesses weak and strong acid sites, both of which are derived from P(OH) groups [16]. The Lewis acid centers could be attributed to Zr^{4+}, as suggested by Spielbauer et al. [17].

3,3-Diphenyl-3H-naphtho [18, 19] pyrans or naphthopyrans are well-known as photochromic chromenes which demonstrate a unique enviable photochromic properties [18] and have attractive topic of passionate investigations intended for mounting novel materials with useful applications in the industrial marketplace. For expedient access to designed photochromic materials based on this structural pattern, it is dominant that dependable, alternative and general synthetic pathways be willingly accessible. However, the various synthetic routes for the synthesis of 3,3-diphenyl-3H-naphtho [18, 19] pyrans, diaryl benzopyrans and naphthopyrans

are limited with respect to the yield and scope [19–21]. The building of the 3,3-diphenyl-3*H*-naphtho [18, 19] pyrans can be achieved by a "one-pot reaction" starting from a suitable bis-naphthol and the commercially available 1,1-diphenyl-2-yn-1-ol [22, 23].

In the work described in this paper, we introduce a simple and rapid one-step method for the synthesis of solid acidic catalysts of mesoporous zirconium and tin phosphate. Different tools were used in the characterization of the catalysts such as XRD, FT-IR, SEM, TEM, N_2 adsorption. The catalytic activity of the prepared catalysts was tested for the synthesis of photochromic bis-naphthopyran via the Claisen rearrangement.

Experimental

Catalyst preparation

The zirconium phosphate catalysts (ZrP) were prepared following procedures previously reported [13], which consisted of preparation of $ZrOCl_2{\cdot}8H_2O$ and $NH_4H_2PO_4$ solutions. Then, $NH_4H_2PO_4$ was added dropwise to $ZrOCl_2{\cdot}8H_2O$ solution under vigorous stirring at a molar ratio of Zr:P = 1:2 (ZrP2). The solution was stirred at room temperature for 3 h. The mixture was aged under ambient conditions for 12 h. The precipitate was washed with deionized water until free of chloride ions and the pH was neutral. The precipitate was then filtered, and dried overnight at 100 °C. The catalyst was powdered and calcined at 400 °C for 4 h in air prior to use. The other two zirconium phosphate catalysts (ZrP1 and ZrP3) were prepared following the same procedure but varying the molar ratio of Zr:P to 1:1 and 1:3 respectively.

The tin phosphate catalyst (SnP1) was obtained by preparing two aqueous solutions of $SnCl_4{\cdot}5H_2O$ and $NH_4H_2PO_4$. Then the aqueous solution of ammonium dihydrogen phosphate was added drop wise to under vigorous stirring to tin tetrachloride solution at a molar ratio of Sn:P = 1:1 (SnP1). The solution was stirred at room temperature for 3 h. The mixture was aged under ambient conditions for 12 h. The gel was washed with deionized water until free of chloride ions and the pH was neutral. The gel was then filtered, and dried overnight at 100 °C. The catalyst was powdered and calcined at 400 °C for 4 h in air prior to reaction. The other two tin phosphate catalysts (SnP2 and SnP3) were prepared following the same procedure but varying the molar ratio of Sn:P to 1:2 and 1:3, respectively.

Catalyst characterization

Elemental analysis was carried out by inductive coupled plasma ICP-AES (Labtam, 8440 Plasmalab) to determine the actual amounts of phosphorus, zirconium, and tin present in the solid acid catalysts.

X-ray powder diffraction patterns of samples were determined using an X'Pert Philips Materials Research Diffractometer. The patterns were run with copper radiation (Cu K_α, $\lambda = 1.5405$ Å) with the second monochromator at 45 kV and 40 mA with a scanning speed of 2° in 2θ/min.

FT-IR spectra of calcined samples were recorded by using a Nicolet-Nexus 670 FTIR spectrophotometer (4 cm^{-1} resolution and 32 scans) in dried KBr (Sigma) pellets and a measuring range of 400–4000 cm^{-1}.

Transmission electron microscope (TEM) images and the particle size were obtained using a Jeol JEM-1230 operated at 120 kV. For TEM images, the sample powder was dispersed in methanol by using ultrasonic radiation for 10 min, and a drop of the suspension was placed onto the carbon-coated copper grids.

Scanning electron microscopy (SEM) and energy-dispersive X-ray spectroscopy (EDS) were carried out using a Quantum DS-130S dual stage electron microscope.

The adsorption isotherms and the specific surface area (S_{BET}) of the various catalysts were determined from nitrogen adsorption studies conducted at −196 °C using a Quantachrome Autosorb-1-C system.

The total acidity of the solid samples was measured by means of potentiometric titration [24–26]. The solid (0.05 g) was suspended in acetonitrile (Merck), and agitated for 3 h. The suspension was then titrated with 0.1 M *n*-butylamine (Merck) in acetonitrile at 0.05 ml/min. The electrode potential variation was measured with an Orion 420 digital A model by using a double-junction electrode. Lewis and Brønsted acid sites present on the surface of the catalyst were determined with FT-IR spectra of adsorbed pyridine. Prior to the pyridine adsorption [24], small portions of the calcined samples were degassed under vacuum at 200 °C for 3 h, followed by suspending in dry pyridine. The excess pyridine was removed by evaporation. The FT-IR spectra of the pyridine-adsorbed samples were obtained using a Nicolet-Nexus 670 FTIR spectrophotometer by mixing 0.005 g of the sample with 0.100 g KBr in a resolution of 4 cm^{-1}, and in a frequency range of 1400–1700 cm^{-1}. The ratio of Brønsted to Lewis acidity was determined based on the method in the literature [27].

Catalytic activity

A 50-ml round bottomed flask was charged with pre activated phosphate catalyst 0.2 g catalyst, 1,1-diphenyl-2-propyn-1-ol (2.10 mmol) and 2,6-dihydroxynaphthalene (1 mmol) in 20 ml acetonitrile as a solvent. The reaction mixture was stirred under N_2 atmosphere for 2 days at room temperature. Samples from the reaction mixture were withdrawn at different time intervals up to 2 days. The composition of the reaction mixture was identified by GC–MS (HP GCD system equipped with FID detector). After the completion of the reaction, the reaction mixture was transferred into 10 ml of ethanol and stirred for 15 min. The catalyst was removed from the reaction mixture by simple filtration.

Results and discussion

Surface area measurements

The textural properties of the catalysts were evaluated by N_2 adsorption–desorption measurements at −196 °C. Table 1 presents a summary of the textural properties of the prepared catalysts such as S_{BET}, mean pore radius and pore volume. The

adsorption–desorption isotherms of zirconium phosphate are shown in Fig. 1. The adsorption–desorption isotherms of tin phosphate and the pore size distribution curves of tin and zirconium phosphate are given in the Supplementary material, Figs. S1 and S2. According to adsorption–desorption isotherms shown in Fig. S1 (Supplementary material), tin phosphate catalysts exhibited type II adsorption isotherm in the IUPAC classifications, with a H3 type hysteresis loop, which is characteristic of the presence of a large proportion of mesopores [28]. The isotherms of these catalysts have a closed hysteresis loops and desorption branches joints the adsorption ones at relative pressure of about 0.30–0.45. The specific surface area of SnP1 was found to be 268.51 $m^2\ g^{-1}$ with an average pore radius of 1.7 nm as listed in Table 1, when the phosphate loading increase up to SnP3 the specific surface area further decreased and the average pore radius was shifted to higher value (4.7 nm).

On the other hand, the adsorption–desorption isotherms of N_2 gas over zirconium phosphate catalysts are shown in Fig. 1. For zirconium phosphate catalysts, the isotherms can be classified as type IV (in the IUPAC classifications) characteristic of mesoporous materials [29] with a H2 type hysteresis loop. Pronounced desorption hysteresis suggests the existence of mesoporous in these materials. The specific area was also found to decrease with phosphate ratio to become 91.72 $m^2\ g^{-1}$ in ZrP3. The average pore size distribution analysis using the BJH method from the desorption part of the isotherm of zirconium phosphate reveals very narrow pore size distribution (Supplementary material, Fig. S2b). Moreover, the average pore size distribution of the samples (Table 1) is in the range of ca. 1.90–1.92 nm, a borderline of micro- and mesoporous regions. Such behavior was previously observed in yttria zirconia and silica zirconia materials [30, 31]. Molina et al. [31] has been termed these as super microporous materials.

XRD patterns

X-ray diffraction was used to study the crystal structure of all prepared phosphate catalysts. In the wide angle XRD patterns of zirconium phosphate catalyst, two broad peaks in 2θ range of 10°–40° and 40°–70° (Supplementary material, Fig. S3b) indicated the amorphous nature of the prepared zirconium phosphate catalysts calcined at 400 °C. The low angle XRD of zirconium phosphate samples did not

Table 1 Surface, textural, and acidic properties of the prepared catalysts

Catalyst	Ratio of M/P	Surface area (m^2/g)	Pore radius (Å)	Pore volume (ccg^{-1})	Ei (mV)	Acid amount (mmol n-butylamine g^{-1})	Ratio of B/L
ZrP1	0.96	193.82	19.28	0.189	+67	0.64	0.834
ZrP2	1.90	144.87	19.14	0.124	+567	1.41	1.061
ZrP3	2.78	91.72	19.08	0.090	+680	1.93	1.210
SnP1	0.94	268.51	17.03	0.393	+37	0.51	0.834
SnP2	1.85	127.21	28.45	0.251	+476	1.67	0.982
SnP3	2.73	66. 72	47.86	0.148	+351	1.55	0.906

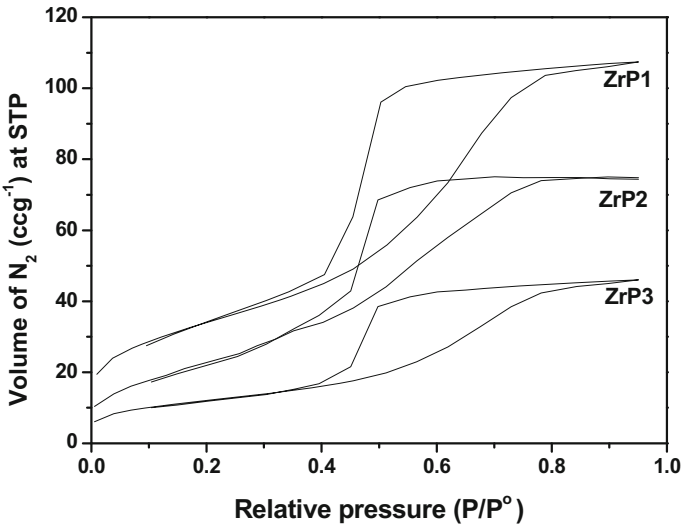

Fig. 1 N_2 adsorption–desorption isotherms at −196 °C of zirconium phosphate catalysts calcined at 400 °C

show any diffraction peaks indicate the formation of mesoporous zirconium phosphate (Supplementary material, Fig. S3a). Moreover, previous studies have shown that the presence of phosphate stabilizes the amorphous zirconia phase [32]. It has also been reported that amorphous zirconium phosphate is thermally stable even after calcination at 800 °C [33].

On the other hand, a single broad peak in low angle XRD patterns for 400 °C calcined tin phosphate catalysts was observed at around $2\theta = 2.2$–2.3, corresponding to a *d*-values of $\sim$4 to 3.8 nm (Supplementary material, Fig. S4a). The single and broad peak at $2\theta = 2.2$–2.3 implies the formation of mesoporous tin phosphate. Sinhamahapatra et al. [34] reported that, the presence of only one broad peak indicates the existence of short range order wormhole-like meso-structure. The wide angle XRD patterns of calcined tin phosphate samples exhibit two broad peak in 2θ range of 10°–40° and 40°–70° (Supplementary material, Fig. S4b) indicating their amorphous nature.

FTIR spectroscopic analysis

The synthesized catalysts were further characterized by FT-IR (Fig. S5, Supplementary material). The FTIR spectra of the materials indicate the presence of phosphate groups by the appearance of bread peak between 800 and 1400 cm^{-1} centered at around 1100 cm^{-1} that is due to $–PO_4$ stretching vibrations [35]. The bands at 3460 and 1630 cm^{-1} are attributed to the asymmetric OH stretching and bending of water molecule, respectively. The band at 2370 cm^{-1} is due to P–O–H stretching responsible for the Brønsted acidity [33]. Moreover, another peak at 750 cm^{-1} is observed, which is attributed to a P-O-P (poly phosphate) like group [34]. This peak is not observed in SnP1 and ZrP1 as seen in Fig. S5, once the phosphate ratio increase

more than 1:1. This peak can be clearly observed especially when the metal: phosphate ratio becomes 1:3. This means that at higher concentrations of phosphate, polyphosphate layers are formed on the catalyst surface, which may affect the acidity of the catalyst.

SEM and TEM

Figs. 2 and 3 represent the SEM and TEM micrographs of SnP2 and ZrP2 samples that calcined at 400 °C, respectively. The SEM photographs of SnP2 and ZrP2 samples are shown in Fig. 2. From the SEM images, it can be seen that the catalysts is composed of some aggregated spherical particles. The images also show that the participation of other particles that have broad size range and an irregular forms or shapes. The lack of a clearly defined morphology may correlates with the low crystallinity of the phosphate catalysts. More SEM images for SnP2 and ZrP2 in the Supplementary material, Fig. S6.

The TEM images of SnP2 and ZrP2 samples are presented in Fig. 3. The TEM images for SnP2 (Fig. 3a) show that there are spherical particles of small diameters aggregated throughout the specimen that give rise to mesopores in the material. A more magnified microgram (Fig. S7a, in the Supplementary material) confirms the presence of worm like pore structures. Similarly, the TEM images of ZrP2 shows spherical particles with diameter around 80.0 nm (Fig. S7, Supplementary material). The connectivity between spherical particles is visible from the micrograph (Fig. S7). This may be due to the condensation reactions among hydroxyl groups on adjacent spherical particles during aging or during calcination, to produce the agglomerates of spherical particles.

Surface acidity

Non aqueous potentiometric titration

The acidities of all the phosphate catalysts were first characterized by nonaqueous potentiometric titration with *n*-butylamine in acetonitrile. Using this technique, it is

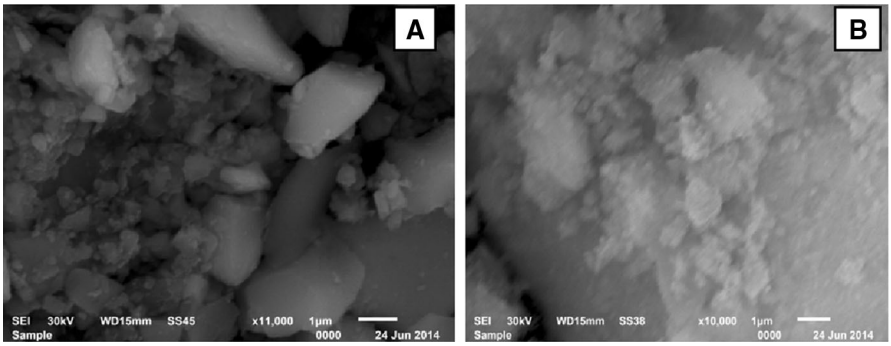

Fig. 2 SEM images of: **a** SnP2, **b** ZrP2 catalysts calcined at 400 °C

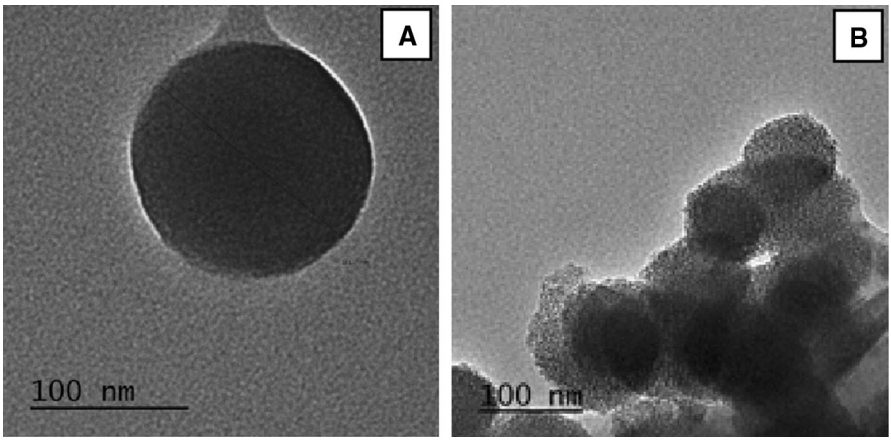

Fig. 3 TEM images of: **a** SnP2, **b** ZrP2, catalysts calcined at 400 °C

possible to estimate the relative strength and the total number of acid sites present in the solids. As a criterion to interpret the results, it was suggested that the initial electrode potential (E_i) indicates the maximum acid strength of the sites according to the following scale: $E_i > 100$ mV (very strong sites), $0 < E_i < 100$ mV (strong sites), $-100 < E_i < 0$ mV (weak sites) and $E_i < -100$ mV (very weak sites) [36].

The titration curves of the catalysts are shown in Figs. S8 and S9 (Supplementary material) and the data are listed in Table 1. According to the above classification, ZrP1 and SnP1 samples exhibit strong acid sites, E_i between 0 and +100 mV, and have also a small number of acid sites (Table 1). When the phosphate amount increased, both the number and strength of acid sites increase. In the case of zirconium phosphate samples, the surface acidity and acid strength increase to maximum at Zr:P ratios 1:3, while in the case of tin phosphate, the sample becomes maximum at Sn:P ratio 1:3 then slightly decrease in the Sn:P ratio 1:3 sample. The results also indicate that the zirconium phosphate samples show higher surface acidity and more acidic sites strength compared to tin phosphate samples. The distribution of excess phosphate species on the surface as multilayers or polyphosphates aggregates may also play an important role in the variation of acidity with phosphate loading.

FTIR spectra of chemisorbed pyridine

To further identify the acid types and ratio of Brønsted (B) and Lewis (L) acidic sites, FT-IR spectra in the spectral region 1700–1400 cm^{-1} of adsorbed pyridine on the samples were collected and presented in Fig. 4. It is clear that all the phosphate catalysts contain mixture of Lewis (L) acid sites and Brønsted (B) acid sites, as indicated by strong IR bands at around 1450 cm^{-1} (L), 1545 cm^{-1} (B) and 1635 cm^{-1} (B) [37]. In addition, the band at 1490 cm^{-1} indicates the formation of the adjacent L and B acid sites. The ratio of Lewis (L) and Brønsted (B) acid sites present in the catalysts were calculated using area under the peak of 1450 cm^{-1}

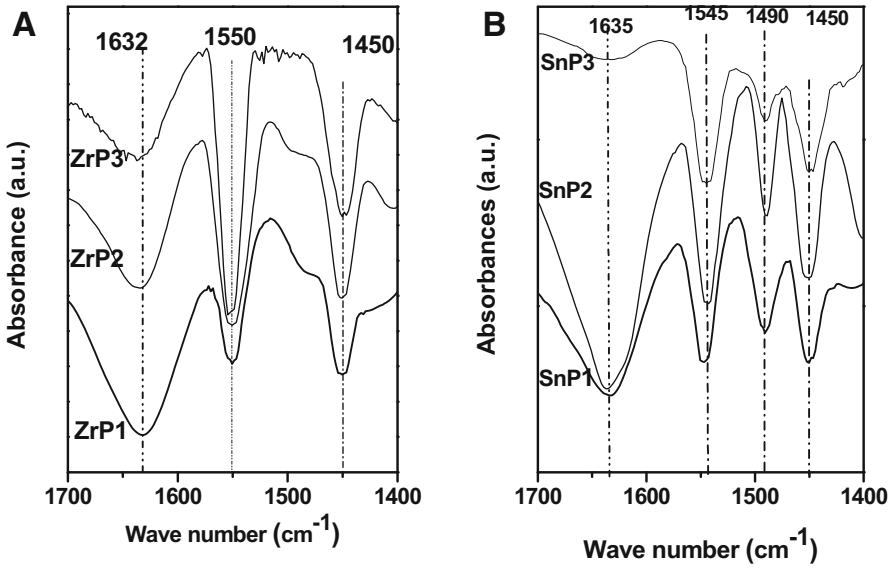

Fig. 4 FT-IR spectra of chemisorbed pyridine over: **a** Zirconium phosphate, **b** tin phosphate catalysts calcined at 400 °C

(due to pyridine at Lewis acid sites) and 1545 (1550) cm^{-1} (due to pyridine at Brønsted acid sites) [27, 38]. The ratios of Brønsted to Lewis (B/L) of all phosphate catalysts are listed in Table 1. As can be seen in Table 1 and Fig. 4a, in the case of zirconium phosphate catalysts, when the phosphate loading increases gradually, the Brønsted acidity also increases up to ZrP3 sample. On the other hand, in the case of tin phosphate samples (Fig. 4b), when the phosphate loading increase from Sn:P ratio 1:1 to 1:2 the Brønsted acidity increases. Further increase of phosphate content (SnP3, Sn:P ratio 1:3) results in small decrease in the Brønsted acidity.

The results of surface acidity measurement indicated that tuning of the phosphate loading in the synthetic process is a promising way to tailor the acidic properties of the resultant catalysts. The Brønsted acid on the surface of the support may be related to the states of PO_x species on the surface, and the hydrated tetrahedral-coordinated PO_4^{3-} species $[(H_2PO_4)^-]$ on the surface were contributed to the Brønsted acid sites [39–41]. While, on the other hand, Lewis acid sites were derived from the tetrahedral MO_4 and octahedral MO_6 species in the framework [42]. In zirconium phosphate catalysts (Fig. 4a and Table 1), the gradual increase of phosphate content was accompanied with gradual increase of P-O–H groups on the surface. The increase of P–O–H groups on the surface causes increase in Brønsted acid sites. While in tin phosphate catalysts, the decrease in the Brønsted acidity in SnP3 may be due to the formation of polyphosphate, as a single or poly-phosphate layer. The formation of a polyphosphate layer occurred through sacrificing two P-O–H groups (responsible for Brønsted acidity) to form P–O–P structures. The superficial formation of poly-phosphate structures may be more effective in SnP3 catalyst due to its smaller surface area.

Catalytic activity

The catalytic activity of the prepared catalysts was tested in the synthesis of photochromic bis-naphthopyran via the Claisen rearrangement at room temperature.

Our preliminary studies in this area focused on the use of 0.1 g of the catalyst calcined at 400 °C in the reaction of 1,1-diphenyl-2-propyn- 1-ol (2.10 mmol) and 2,6-dihydroxynaphthalene (1 mmol) in dry acetonitrile (20 ml) as a solvent under nitrogen atmosphere in absence of light. Under these conditions, the reaction was extremely slow, affording 15 % adduct after 3 days at room temperature. Interestingly, we observed a dramatic improvement in the course of the reaction when 0.2 g of the catalyst was used under the same reaction condition. Moreover, when we increase the reaction temperature to higher values, a notable decrease in the percentage yield of product, this decrease in the product yield may be due to the thermal instability of the reaction mixture at higher temperatures. During this study, the reactions were carried out at room temperature using 0.2 g of the catalyst.

Effect of phosphate loading ratio

Under optimal conditions, treatment of 1,1-diphenyl-2-propyn-1-ol (2.10 mmol) and 2,6-dihydroxynaphthalene (1 mmol) in acetonitrile with 0.2 g of the catalyst at room temperature, calcined at 400 °C for 48 h. The effect of phosphate loading ratios on the percentage yield of the product is shown in Fig. 5. As can be seen, all the catalysts with different phosphate loadings exhibit percentage yield of bis-

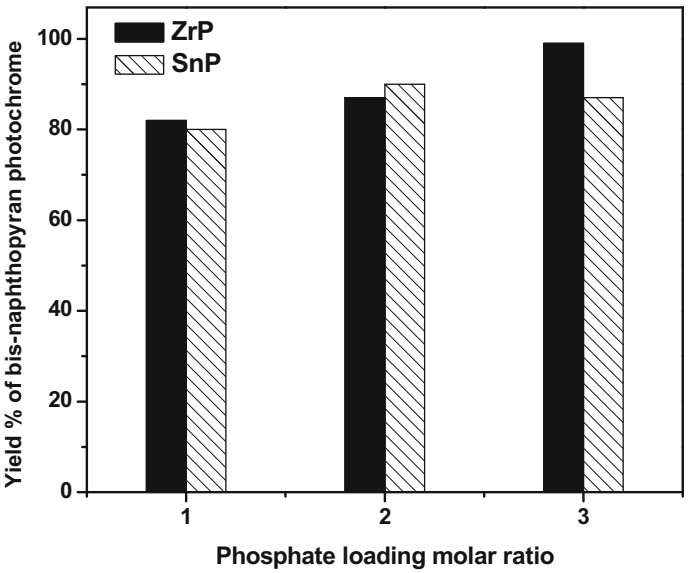

Fig. 5 Effect of phosphate loading over zirconium and tin phosphate on percentage yield of bis-naphthopyran photochrome using 0.2 g catalyst, 1,1-diphenyl-2-propyn-1-ol (2.10 mmol) and 2,6-dihydroxynaphthalene (1 mmol) in 20 ml acetonitrile as a solvent at room temperature after 24 h

naphthopyran photochrome ranging from 82 to 99 % with 100 % selectivity at room temperature. Also, zirconium phosphate catalysts showed higher catalytic activity than tin phosphate catalysts. The trend of catalytic activity using tin and zirconium phosphate as catalysts was similar to catalysts acidity, suggesting that the Brønsted acid sites generated from P–O–H enhanced the product formation.

Effect of reaction time

The effect of reaction time was studied ZrP3 and SnP2 at room temperature using 0.2 g of the catalyst. The results are shown in Fig. 6. As can be seen in Fig. 6, the percentage yield of the product increases gradually with increasing the reaction time till almost constant value after around 24 h. After 24 h the percentage yield of the product becomes almost constant or increases by small amount with further increase in the reaction time, which suggests that, only 24 h are enough for the reaction.

The catalyst filtration test (Fig. S10, Supplementary material) proved heterogeneous nature of catalysis over ZrP2 catalyst after the fast removal of the catalyst at ca. 55.8 % yield and after 10 h, the reaction in the filtrate stopped completely, indicating that no active phosphate species had leached into solution during the reaction. Additionally, elemental analysis confirmed that no phosphate species were present in the filtrate.

Reusability of the catalyst

To study and confirm the reusability of the catalysts, ZrP3 and SnP2 were selected for the reaction over five cycles. The catalysts were recovered by simple filtration

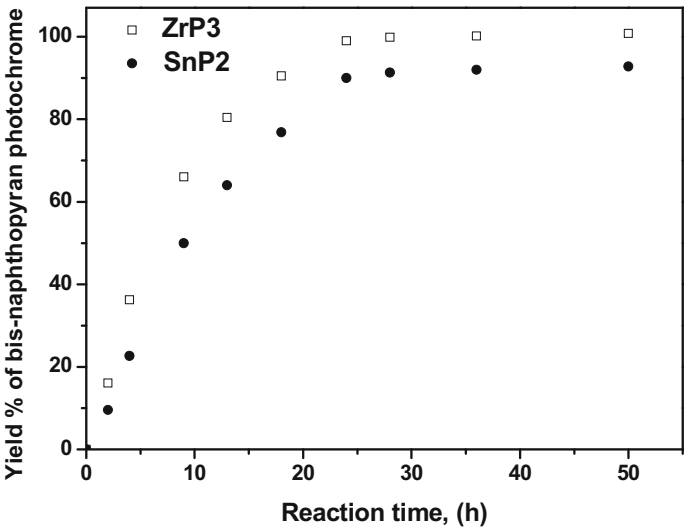

Fig. 6 Effect of reaction time over ZrP3 and SnP2 on percentage yield of bis-naphthopyran photochrome using 0.2 g catalyst, 1,1-diphenyl-2-propyn-1-ol (2.10 mmol) and 2,6-dihydroxynaphthalene (1 mmol) in 20 ml acetonitrile as a solvent at room temperature

and washed with ethanol and dried in air at 100 °C before reuse. The performance of ZrP3 and SnP2 reusability was conducted for the reaction at room temperature for 24 h using 0.2 g of catalyst. As shown in Fig. 7, the catalytic activity of ZrP3 and SnP2 did not decrease significantly after five runs, which demonstrated that ZrP3 and SnP2 were stable in this system. The percentage yield maintained at around 99 and 90 % for ZrP3 and SnP2 respectively until the fifth run. The limited decrease in the catalytic activity may be due to gradual loss of the catalyst during filtration process.

As shown in Scheme 1 (Supplementary material), the Brønsted acidity is the main factor that may control the reaction. The yield obtained under the conditions describes herein offer considerable improvement over those previously reported [22, 23]. The unique advantages of the method can be appreciated in the preparation of bis-naphthopyran derivatives, which have otherwise been previously obtained in only low yields [22, 23]. Many authors [18, 22, 23, 43] prepared bis-naphthopyran derivatives by using *para* toluene sulfonic acid as homogeneous catalyst, the percentage yield of the product were less than 45 % after 48–72 h of the reaction at room temperature in addition to it was very hard to obtain the product in pure form. Under the conditions reported herein, an excellent yield of bis-naphthopyran derivatives was obtained, and analytically pure bis-naphthopyran could be obtained by simple filtration of the cold reaction mixture in 24 h using 0.2 g of the catalyst. The acid-catalyzed mechanism for the formation of the bis-naphthopyrans involves the following two steps. First, 1,1-diphenyl-2-propyn-1-ol and 2,7-dihydoxy naphthalene are condensed to give propargyl ether in the presence of metal phosphate as source of H^+ Brønsted acid catalysts. In the second step, the Claisen rearrangement of propargyl ether occurred to give some intermediate shown in

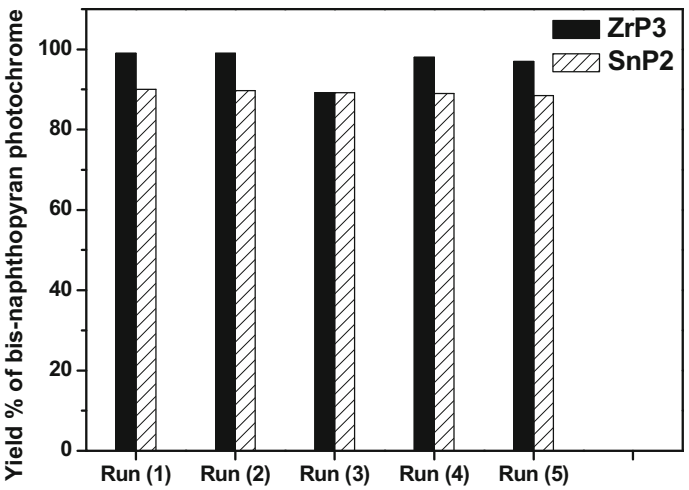

Fig. 7 Reusability of ZrP3 and SnP2 for the production of bis-naphthopyran photochrome using 0.2 g catalyst, 1,1-diphenyl-2-propyn-1-ol (2.10 mmol) and 2,6-dihydroxynaphthalene (1 mmol) in 20 ml acetonitrile as a solvent at room temperature after 24 h

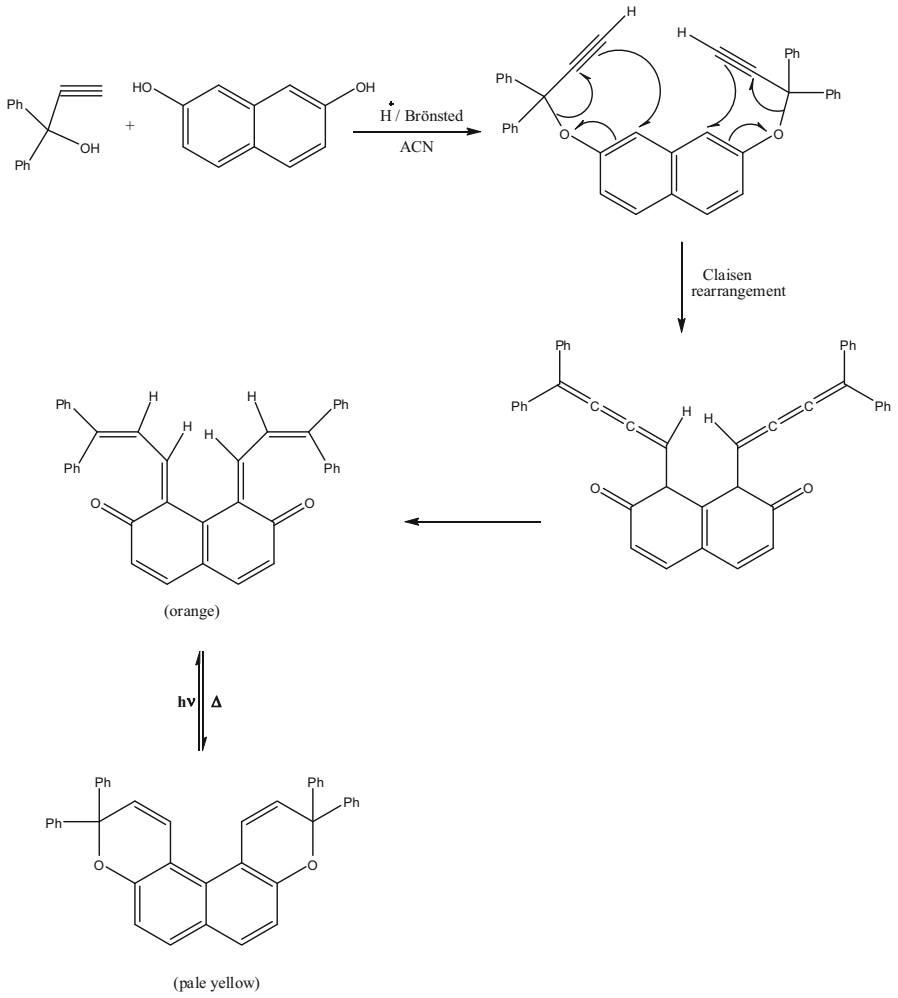

Scheme 1 Possible reaction mechanism

Scheme 1 (see supplementary materials), and finally bis-naphthopyrans was obtained via cyclization of quinodimethane intermediate in excellent yields.

Conclusion

In conclusion, we report a superficial and efficient one step method for the synthesis of highly active mesoporous zirconium and tin(IV) phosphate. The catalysts were characterized using imaging, textural and spectroscopic techniques. The results showed that in the case of zirconium phosphate samples, the surface acidity and Brønsted ratio increase to maximum at Zr:P ratio 1:3, while in the case of tin

phosphate, the sample becomes maximum at Sn:P ratio 1:2 then slightly decrease in Sn:P ratio 1:3 sample. The results also indicate that the zirconium phosphate samples show higher surface acidity and more Brønsted acid sites compared to tin phosphate samples. Also, the samples with higher ratio of Brønsted acid sits namely, SnP2 and ZrP3 exhibit higher catalytic activities of 90 and 98 %, respectively. Moreover, the values of pore radius and pore volume listed in Table 1 are wide enough to make the acid sites inside the porous accessible to the reactants molecules. We have developed a facile one-pot synthesis of photochromic bis-napthopyran via the Claisen rearrangement using our solid acid catalysts. The product was obtained with 100 % selectivity at room temperature in N_2 atmosphere after 24 h. The method can permit expedient admittance to a wide range of photochromic pyrans systems that have been previously accessed in poor yields with purification difficulties.

References

1. Lyon CJ, Sarsani VR, Subramaniam B (2004) Ind Eng Chem Res 43:4809
2. Liu Y, Guan Y, Li C, Lian J, Gan GJ, Lim EC, Kooli F (2006) J Catal 244:17
3. Rosenberg DJ, Bachiller-Baeza B, Dines TJ, Anderson JA (2003) J Phys Chem B 107:6526
4. Izumi Y, Urabe K, Onaka M (1992) Zeolite, clay, and heteropoly acid in organic reactions. VCH, Weinheim
5. Sheldon RA, Van Bekkum H (2001) Fine chemicals through heterogeneous catalysis. Wiley-VCH, Weinheim
6. Wang SB, James AG (2000) Chem Commun 24:2499
7. Srivastava R, Iwasa N, Fujita SI, Arai M (2008) Chem Eur J 14:9507
8. Clearfield A (1982) Inorganic ion exchange materials. CRC Press, Boca Raton
9. La Ginestra A, Patrono P, Berardelli ML, Galli P, Ferragina C, Massucci MA (1987) J Catal 103:346
10. Costa MCC, Johnstone RAW, Whittaker D (1995) J Mol Catal A 103:155
11. Ginestra AL, Patrono P (1987) Mater Chem Phys 17:161
12. Patel SM, Chudasama UV, Ganeshpure PA (2002) React Kinet Catal Lett 76:317
13. Kamiya Y, Sakata S, Yoshinaga Y, Ohnishi R, Okuhara T (2004) Catal Lett 94:45
14. Srilakshmi C, Ramesh K, Nagaraju P, Lingaiah N, Prasad PSS (2006) Catal Lett 106:115
15. Rao KN, Sridhar A, Lee AF, Tavener SJ, Young NA, Wilson K (2006) Green Chem 8:790
16. Hattori T, Ishiguro A, Murakami Y (1978) J Inorg Nucl Chem 40:1107
17. Spielbauer D, Mekhemer GAH, Riemer T, Zaki MI, Knözinger H (1997) J Phys Chem B 101:4681
18. Gemert BV (1999) In: Crano JC, Guglielmetti RJ (eds) Organic photochromic and thermochromic compounds: main photochromic families, vol. 1, chapter 3. Plenum Press, New York
19. Gabbutt CD, Hartley DJ, Hepworth JD, Heron BM, Kanjia M, Rahman M (1994) Tetrahedron 50:2507
20. Cottam J, Livingstone R (1965) J Chem Soc 6646
21. Hara T (1998) US Patent 5808100
22. Tanaka K, Aoki H, Hosomi H, Ohba S (2000) Org Lett 2(14):2133
23. Zhao W, Carreira EM (2006) Org Lett 8(1):99
24. Rao KN, Reddy KM, Lingaiah N, Suryanarayana I, Sai PS, Prasad J (2006) Appl Catal A 300:139
25. Khder AS, Hassan HMA, El-Shall MS (2012) Appl Catal A 412:77
26. Khder AS, Hassan HMA, El-Shall MS (2014) Appl Catal A 487:110
27. Ramli ANAS, Amin NAS (2015) J Mole Catal A Chem 407:113
28. Ahmed AI, El-Hakam SA, Khder AS, El-Yazeed WSA (2013) J Mole Catal A Chem 366:99
29. Paul M, Pal N, Rana BS, Sinha AK, Bhaumik A (2009) Catal Commun 10:2041
30. Mamak M, Coombs N, Ozin G (2000) J Am Chem Soc 122:8932
31. Molina AI, Robles JM, Torres PM, Finocchio E, Busca G, Castellón ER, Fierro JLG, López AJ (2004) Micropor Mesopor Mater 75:23

32. Ciesla U, Schacht S, Stucky GD, Unger KK, Schüth F (1996) Angew Chem Int Ed Engl 35:541
33. Sinhamahapatra A, Sutradhar N, Roy B, Tarafdar A, Bajaj HC, Panda AB (2010) Appl Catal A 385:22
34. Sinhamahapatra A, Sutradhar N, Roy B, Pal P, Bajaj HC, Panda AB (2011) Appl Catal B Envir 103:378
35. Rao CNR (1963) Chemical applications of infrared spectroscopy. Academic Press, New York
36. Cid R, Pecci G (1985) Appl Catal A Gen 14:15
37. Escribano VS, Panizza M, Carnasciali MM, Busca G (2001) J Mater Chem 11:1891
38. Tyagi B, Chudasama CD, Jasra RV (2006) Appl Clay Sci 31:16
39. Yang FL, Liu QS, Bai XF, Du YG (2011) Bioresour Technol 102:3424
40. Kapoor MP, Inagaki S, Yoshida H (2005) J Phys Chem B 109:9231
41. Nakayama H, Eguchi T, Nakamura N, Yamaguchi S, Danjyo M, Tsuhako M (1997) J Mater Chem 7:1063
42. Nakajima K, Baba Y, Noma R, Kitano M, Kondo JN, Hayashi S (2011) J Am Chem Soc 133:4224
43. BKnowles D, Gemert BV (1995) US Patent 5,464,567